

# A chiral quark-soliton model with broken scale invariance for nuclear matter

Alessandro Drago and Valentina Mantovani Sarti

*Dipartimento di Fisica, Università di Ferrara and INFN, Sez. Ferrara, 44100 Ferrara, Italy*

We present a model for describing nuclear matter at finite density based on quarks interacting with chiral fields,  $\sigma$  and  $\pi$ . The chiral Lagrangian includes a logarithmic potential, associated with the breaking of scale invariance. We provide results for the soliton in vacuum and at finite density, using the Wigner-Seitz approximation. We show that the model can reach higher densities respect to the linear- $\sigma$  model and we estimate how a few observables evolve with the density.

PACS numbers: 12.39.Fe, 21.65.Mn, 21.30.Fe

## I. INTRODUCTION

The problem of studying nuclear matter with chiral Lagrangians is not trivial; for instance models based on the linear  $\sigma$ -model fail to describe nuclear matter already at  $\rho \sim \rho_0$  because the normal solution in which chiral symmetry is broken becomes unstable respect to the Lee-Wick phase. In Ref. [1] Furnstahl and Serot conclude that the failure of the  $\sigma$ -model is due to the restrictions on the scalar field dynamics imposed by the Mexican hat potential. A possible solution to this problem is still to use a linear realization, but with a new potential, which includes terms not present in the Mexican hat potential. A guideline in building such a potential is scale invariance [2–5].

In QCD the invariance under dilatation is spontaneously broken due to the presence of the parameter  $\Lambda_{QCD}$  coming from the renormalization process. Formally, the non conservation of the dilatation current is strictly connected to a not vanishing gluon condensate:

$$\langle \partial_\mu j_{QCD}^\mu \rangle = \frac{\beta(g)}{2g} \langle F_{\mu\nu}^a(x) F^{a\mu\nu}(x) \rangle. \quad (1)$$

In the approach of Schechter [6], Migdal, and Shifman [7] a scalar field representing the gluon condensate is introduced and its dynamics is regulated by a potential chosen so that it reproduces (at mean-field level) the divergence of the scale current that in QCD is given by Eq. (1). The potential of the dilaton field is therefore determined by the equation:

$$\theta_\mu^\mu = 4V(\phi) - \phi \frac{\partial V}{\partial \phi} = 4\epsilon_{vac} \left( \frac{\phi}{\phi_0} \right)^4 \quad (2)$$

where the parameter  $\epsilon_{vac}$  represents the vacuum energy. To take into account massless quarks a generalization was proposed in Ref. [8], so that also chiral fields contribute to the trace anomaly. In this way the single scalar field of Eq. (2) is replaced by a set of scalar fields  $\{\sigma, \pi, \phi\}$ .

It has already been shown that an hadronic model based on this dynamics provides a good description of nuclear physics at densities about  $\rho_0$  and it describes the gradual restoration of chiral symmetry at higher densities [9]. In the same work the authors have shown a phase diagram, where the interplay between chiral and

scale invariance restoration lead to a scenario similar to that proposed by McLerran and Pisarski in [10]. This is not too surprising since the large  $N_c$  limit explored in [10] should be well represented in chiral models as the one discussed in [9]. It is therefore tempting to explore the scenario presented in [9] at a more microscopic level.

*The new idea we develop in this work is to interpret the fermions as quarks, to build the hadrons as solitonic solutions of the fields equations as in [11, 12] and, finally, to explore the properties of the soliton at finite density using the Wigner-Seitz approximation.*

Similar approaches to a finite density system have been investigated in the past [13–19]. A problem of those works is that the solitonic solutions are unstable and disappear already at moderate densities when e.g. the linear  $\sigma$ -model is adopted [18]. We are therefore facing an instability similar to the one discussed and solved when studying nuclear matter with hadronic chiral Lagrangians. *The main aim of our work is to check whether the inclusion of the logarithmic potential allows the soliton crystal to reach higher densities.*

We should remark that this model has already been studied at zero density in [20], but using a different technique to describe the single nucleon. Instead no calculation exists at finite density.

The structure of the paper is as follows. In Sec. II we describe the model we are using, in Sec. III we review the mean-field approximation and the hedgehog ansatz. Next in Sec. IV we present results for the soliton in vacuum at mean-field level and by adopting a projection technique. In Sec. V we show the results for the Wigner-Seitz lattice of solitons. Finally, in Sec. VI we present our conclusions and future outlooks.

## II. THE MODEL

In a chiral quark-soliton model quarks are coupled to mesons in a chirally invariant way. Following Refs. [2–5, 9] we consider the Lagrangian:

$$\begin{aligned} \mathcal{L} = & \bar{\psi} (i\gamma^\mu \partial_\mu - g(\sigma + i\boldsymbol{\pi} \cdot \boldsymbol{\tau} \gamma_5)) \psi \\ & + \frac{1}{2} (\partial_\mu \phi \partial^\mu \phi + \partial_\mu \sigma \partial^\mu \sigma + \partial_\mu \boldsymbol{\pi} \cdot \partial^\mu \boldsymbol{\pi}) \\ & - V(\phi, \sigma, \pi). \end{aligned} \quad (3)$$

Here  $\psi$  is the quark field,  $\sigma$  and  $\pi$  are the chiral fields and  $\phi$  is the dilaton field which, in the present calculation, is kept frozen at its vacuum value  $\phi_0$ .

The potential is given by:

$$V(\phi, \sigma, \pi) = B\phi_0^4 \left( \ln \frac{\phi}{\phi_0} - \frac{1}{4} \right) - \frac{1}{2} B\delta\phi^4 \ln \frac{\sigma^2 + \pi^2}{\sigma_0^2} + \frac{1}{2} B\delta\phi^2 \frac{\phi_0^2}{\sigma_0^2} \left( \sigma^2 + \pi^2 - \phi^2 \frac{\sigma_0^2}{2\phi_0^2} \right) - \frac{1}{4} \epsilon_1 \left( \frac{\phi}{\phi_0} \right)^2 \left[ \frac{4\sigma}{\sigma_0} - 2 \left( \frac{\sigma^2 + \pi^2}{\sigma_0^2} \right) - \left( \frac{\phi}{\phi_0} \right)^2 \right] - V_0 \quad (4)$$

where the logarithmic term generates from (2). The first two terms of the potential are responsible for the breaking of scale invariance, while the second line is needed to ensure that in the vacuum  $\phi = \phi_0$ ,  $\sigma = \sigma_0$  and  $\pi = 0$ , i.e it provides spontaneous symmetry breaking. The last line explicitly breaks the chiral invariance of the lagrangian, giving mass to the pion.

The constants  $B$  and  $\phi_0$  can be fixed by choosing a value for the mass of the glueball and for the vacuum energy  $\epsilon_{vac}$ , while  $\delta = 4/33$  is provided by the QCD beta function and it corresponds to the relative weight of the fermionic and of the gluonic degrees of freedom. Finally the constant  $V_0$  ensures that the potential energy is vanishing in the vacuum.

As anticipated, we choose to keep the dilaton field frozen. This decision (which obviously simplifies the dynamics of the system) can be justified by the results obtained in [3, 9], where it has been shown that at low temperatures the dilaton remains close to its vacuum value even at large densities. Therefore the degrees of freedom of our model are limited to quarks, pion and sigma similarly to the linear  $\sigma$ -model whose solitonic solutions have been obtained in [11]. The potential can be written in a simpler form and it reads:

$$V(\sigma, \pi) = \lambda_1^2 (\sigma^2 + \pi^2) - \lambda_2^2 \ln(\sigma^2 + \pi^2) - \sigma_0 m_\pi^2 \sigma \quad (5)$$

where:

$$\lambda_1^2 = \frac{1}{2} \frac{B\delta\phi_0^4 + \epsilon_1}{\sigma_0^2} = \frac{1}{4} (m_\sigma^2 + m_\pi^2) \quad (6)$$

$$\lambda_2^2 = \frac{1}{2} B\delta\phi_0^4 = \frac{\sigma_0^2}{4} (m_\sigma^2 - m_\pi^2) \quad (7)$$

$$\epsilon_1 = m_\pi^2 \sigma_0^2. \quad (8)$$

Here the vacuum value  $\sigma_0$  is fixed to be equal to  $f_\pi = 93$  MeV and  $m_\pi = 139.6$  MeV. Besides the quark-pion coupling constant, for which we will use the typical value  $g = 5$  [8, 11], the only parameter left is the sigma mass  $m_\sigma$ . In our work we will mainly investigate  $m_\sigma = 550$  MeV, which is a typical value used in nuclear physics if the sigma has to provide the intermediate range attraction.

It is interesting to compare the logarithmic with the Mexican hat potential. In Fig. 1 it can be seen that in

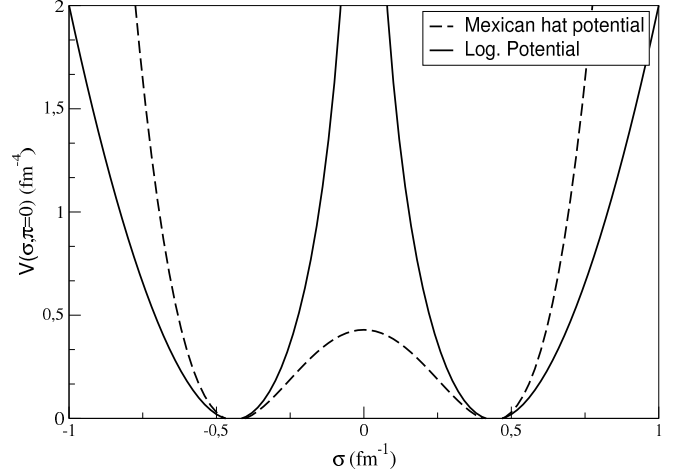


Figure 1: Comparison between the logarithmic (solid line) and the Mexican hat potential (dashed line).

the case of the Mexican hat potential it is relatively easy to restore chiral symmetry by climbing the maximum located at the center. This is not possible in the case of the logarithmic potential as long as the dilaton field remains frozen. Since only at large temperatures the dilaton field changes significantly [9] we can expect that at large densities and moderate temperatures this model provides more stable solitonic solutions. This is the crucial question which will be investigated in our paper.

### III. MEAN-FIELD AND HEDGEHOG ANSATZ

The Euler-Lagrangian equations that follow from the Lagrangian given in eq. (3) read:

$$\begin{aligned} [i\partial\!\!\!/ - g_\pi(\sigma + i\boldsymbol{\pi} \cdot \boldsymbol{\tau}\gamma_5)]\psi &= 0, \\ \partial_\mu \partial^\mu \sigma &= -g\bar{\psi}\psi - \frac{\partial V}{\partial \sigma}, \\ \partial_\mu \partial^\mu \boldsymbol{\pi} &= -ig\bar{\psi}\boldsymbol{\tau}\gamma_5\psi - \frac{\partial V}{\partial \boldsymbol{\pi}}. \end{aligned} \quad (9)$$

The previous equations are relations between quantum fields. The starting point of our calculation is the Mean-Field approximation, where mesons are described by time-independent, classical fields and where powers and products of these fields are replaced by powers and products of their expectation values. The quark spinor in the spin-isospin space is:

$$\psi = \frac{1}{\sqrt{4\pi}} \begin{pmatrix} u(r) \\ iv(r)\boldsymbol{\sigma} \cdot \hat{\mathbf{r}} \end{pmatrix} \chi_h \quad (10)$$

where the spinor  $\chi_h$ , defined as:

$$\chi_h = \frac{1}{\sqrt{2}} (\chi_u \chi_d - \chi_d \chi_u) \quad (11)$$

satisfies the condition for the Grand Spin  $\mathbf{G} = \mathbf{I} + \mathbf{J}$ :

$$\mathbf{G}\chi_h = 0. \quad (12)$$

The hedgehog baryon  $|B\rangle = |N_c q\rangle|\sigma\rangle|\pi\rangle$  is given by the product of quarks and coherent states of mesons fields and it corresponds to a linear combination of states with  $I = 1/2$  and  $I = 3/2$ :

$$|B\rangle = \sum_{JMM_I} (-)^{J+M} c_{J\delta_{M,-M_I}} |J = I, M = -I_3, M_I\rangle. \quad (13)$$

An explicit expression for the coefficients  $c_J$  will be given in Sec. IV B.

It can be shown that the hedgehog state is one of the elements of an infinite class of degenerate solutions of field equations at mean-field level [21].

In particular, the profiles of the chiral fields are related to the hedgehog state by the relations:

$$\frac{\langle B|\sigma|B\rangle}{\langle B|B\rangle} = \sigma_h(r), \quad \frac{\langle B|\pi_a|B\rangle}{\langle B|B\rangle} = \hat{r}_a h(r).$$

Using the mean-field approximations the total energy of the system becomes:

$$\begin{aligned} E = & 4\pi \int r^2 dr \left\{ \frac{3}{4\pi} \left[ u \frac{\partial v}{\partial r} - v \frac{\partial u}{\partial r} + \frac{2uv}{r} \right. \right. \\ & \left. \left. + g\sigma_h(u^2 - v^2) - 2ghuv \right] \right. \\ & \left. + \frac{1}{2} \left[ \left( \frac{\partial \sigma_h}{\partial r} \right)^2 + \left( \frac{\partial h}{\partial r} \right)^2 + \frac{2}{r^2} h^2 + m_\pi^2 h^2 \right] \right. \\ & \left. + V(\phi_0, \sigma_h, h) \right\}. \end{aligned} \quad (14)$$

#### IV. SINGLE SOLITON IN VACUUM

We start by showing how the solitonic solutions for the single nucleon can be built and we check that it is possible to provide a reasonable description of the single nucleon properties with the chosen parameter set.

##### A. Mean-Field approximation

At mean-Field level the chiral fields are classical and the differential equations governing their dynamics have to be supplemented by the appropriate boundary conditions. For the single nucleon case we impose the following boundary conditions to the fields:

$$\begin{aligned} u'(0) &= v(0) = 0, \\ \sigma'_h(0) &= h(0) = 0 \end{aligned} \quad (15)$$

while at infinity the boundary conditions read:

$$\begin{aligned} \sigma_h(\infty) &= \sigma_0, \quad h(\infty) = 0, \\ \frac{v(\infty)}{u(\infty)} &= \sqrt{\frac{-g\sigma_0 + \varepsilon}{-g\sigma_0 - \varepsilon}}, \end{aligned} \quad (16)$$

Table I: Various nucleon properties at mean-field level in the present work and in the  $\sigma$ -model.

Quantity	Log. Model	$\sigma$ -Model	Exp.
$M$ (MeV)	1176	1136	1085
$\langle r_e^2 \rangle_{I=0}$	$(0.73 \text{ fm})^2$	$(0.78 \text{ fm})^2$	$(0.72 \text{ fm})^2$
$\langle r_e^2 \rangle_{I=1}$	$(1.28 \text{ fm})^2$	$(1.32 \text{ fm})^2$	$(0.88 \text{ fm})^2$
$\mu_{I=1} (\mu_N)$	3.83	3.63	4.70
$\langle r_m^2 \rangle_{I=1}$	$(1.12 \text{ fm})^2$	$(1.14 \text{ fm})^2$	$(0.80 \text{ fm})^2$
$g_A$	1.27	1.22	1.26
$\overline{N}_\pi$	2.4	1.9	/

Table II: Contributions to the soliton total energy at mean-field level in the Logarithmic model and in the Linear  $\sigma$ -model. All quantities are in MeV.

Quantity	Log. Model	Linear $\sigma$ -Model
Quark eigenvalue	83.1	107.4
Quark kinetic energy	1138.0	1056.9
$E_\sigma$ (mass+kin.)	334.5	320.3
$E_\pi$ (mass+kin.)	486.0	373.1
Potential energy $\sigma - \pi$	105.7	120.7
$E_{q\sigma}$	-101.4	-62.3
$E_{q\pi}$	-787.0	-673.2
Total energy	1175.6	1136.2

where  $\varepsilon$  is the quark eigenvalue.

A test of the numerical accuracy of the solution originates from another way of expressing the energy, obtained by Rafelski [22] by integrating out the fermionic fields:

$$E_{Raf.} = \int_0^R d^3r \left[ 4 \left( V - \sigma_h \frac{\partial V}{\partial \sigma_h} - h \frac{\partial V}{\partial h} \right) \right]. \quad (17)$$

Our solutions satisfy this consistency test up to a precision of the order of  $10^{-3}$ .

In Table I we present the static properties of the hedgehog baryon at mean-field level and we compare them with results obtained in the linear  $\sigma$ -model [23]. In Table II we show the decomposition of the soliton total energy in its various contributions and again we compare with the linear  $\sigma$ -model [23].

##### B. Projection

The hedgehog baryon defined in section III is not an eigenstate of isospin and angular momentum. Moreover this semi-classical solution also breaks the translational symmetry of the Lagrangian, since the localized soliton is not an eigenstate of the linear momentum, either. In this work we restore the invariance under rotations by

using the projection technique developed in [11, 24]. Instead, we will not restore the translational invariance of our soliton. The spin-isospin eigenstates are defined as follows:

$$|JMM_I\rangle = N_{JM_I} \int d^3\Omega D_{M,-M_I}^J(\Omega)^* \hat{R}(\Omega)|B\rangle \quad (18)$$

where the weight functions  $D$  are the Wigner functions,  $\hat{R}(\Omega)$  is a spatial rotation through Euler angles  $\Omega \equiv (\alpha, \beta, \gamma)$  and  $N_{JM_I}$  is a normalization factor. Since the hedgehog states are eigenstates of the Grand Spin  $\mathbf{G}$ , it is equivalent to rotate either in spin or in isospin space. Moreover, when studying diagonal matrix elements of nucleon states, it is customary to work with states where the third component of the angular momentum  $M$  is equal to  $-M_I$  since in this case the expression of the Wigner function is particularly simple. In this way the projection operator becomes:

$$P_{JM} = \frac{2J+1}{8\pi^2} \int d^3\Omega D_{M,M}^J(\Omega)^* \hat{R}(\Omega). \quad (19)$$

The normalization factor has been determined by using (18)-(19):

$$N_{J,-M}^2 = \left( \frac{2J+1}{8\pi^2} \right)^2 (\langle B|P_{JM}|B\rangle)^{-1}. \quad (20)$$

Finally, the coefficients  $c_J$  in eq. (13) are given by the expression:

$$\begin{aligned} c_J^2 &= \langle B|P_{JM}|B\rangle \\ &= \frac{2J+1}{8\pi^2} \int d^3\Omega \Omega D_{M,M}^J(\Omega) \langle B|\hat{R}(\Omega)|B\rangle. \end{aligned} \quad (21)$$

More details about this technique can be found in [11].

### C. Projected observables

The formalism needed to compute most of the observables can be found in [11, 25]. The only quantity for which we need to provide a new explicit expression is the energy, since in our potential there is a logarithmic term, not present in the  $\sigma$  model.

The energy of the projected state with spin  $J$  reads:

$$\begin{aligned} E_J &= \langle JM - M | : H : | JM - M \rangle \\ &= 4\pi \int r^2 dr \left\{ \frac{3}{4\pi} \left[ u \frac{\partial v}{\partial r} - v \frac{\partial u}{\partial r} + \frac{2uv}{r} \right. \right. \\ &\quad \left. \left. + g(u^2 - v^2)\sigma_h - 2ghuv \right] + \frac{1}{2} \left( \frac{\partial \sigma_h}{\partial r} \right)^2 \right. \\ &\quad \left. + \left[ \left( \frac{\partial h}{\partial r} \right)^2 + \frac{2}{r^2} h^2 + m_\pi^2 h^2 \right] C_0(J, \bar{N}_\pi) \right\} \\ &\quad + \langle JM - M | : \int d^3r V(\sigma_h, h) : | JM - M \rangle \end{aligned} \quad (22)$$

Table III: Projected nucleon properties in the present work and in the linear  $\sigma$ -model and comparison with experimental values.

Quantity	Log. Model	$\sigma$ -Model	Exp.
$E_{1/2} (MeV)$	1075	1002	
$M_N (MeV)$	960	894	938
$E_{3/2} (MeV)$	1140	1075	
$M_\Delta (MeV)$	1032	975	1232
$\langle r_E^2 \rangle_p (fm^2)$	0.82	0.92	0.74
$\langle r_E^2 \rangle_n (fm^2)$	-0.03	-0.01	-0.12
$\langle r_M^2 \rangle_p (fm^2)$	0.82	0.87	0.74
$\langle r_M^2 \rangle_n (fm^2)$	0.86	0.90	0.77
$\mu_p (\mu_N)$	3.00	3.24	2.79
$\mu_n (\mu_N)$	-2.60	-2.50	-1.91
$g_a$	1.52	1.10	1.26
$\langle N_\pi \rangle_J$	1.6 ( $J = 1/2$ )	1.2 ( $J = 1/2$ )	/
	2. ( $J = 3/2$ )	1.6 ( $J = 3/2$ )	

where  $C_0(J, \bar{N}_\pi)$  is a projection coefficient depending on the spin and on the average number of pions  $\bar{N}_\pi$  in the unprojected state. More details about the calculation of the potential term are given in the Appendix.

To compute the static observables we have used the explicit formulae given in the Appendix of Ref. [25]; in addition to radii and magnetic moments we also show the results for the average number of pions in the projected state, given by:

$$\langle N_\pi \rangle_J = \bar{N}_\pi C_0(J, \bar{N}_\pi). \quad (23)$$

As already mentioned before, we do not perform a projection on the linear momentum, but we adopt an easier approach [26] which provides a rough estimate of the center-of-mass corrections to the baryon total energy. The masses for the  $N$  ( $J = 1/2$ ) and for the  $\Delta$  ( $J = 3/2$ ) are then given by:

$$M_J = (E_J - \mathbf{P}^2)^{1/2}. \quad (24)$$

It is important to remark that our results are consistent with the ones obtained in [20]. There, a different approach based on the coherent pair approximation was used. Their results are similar to ours when the coherence length parameter  $x$  is taken to be of the order of one, as suggested in [27]. Finally it should be noticed that the values of most of the observables when computed in the logarithmic model turn out to be slightly closer to the experimental ones than in the case of the  $\sigma$  model.

## V. WIGNER-SEITZ APPROXIMATION TO NUCLEAR MATTER

In order to describe a soliton system at finite density we use the Wigner-Seitz approximation. This approach is very common and it has already been widely applied to both non-linear [14, 15, 19] and linear- $\sigma$  models [18]. Specifically, the Wigner-Seitz approximation consists of replacing the cubic lattice by a spherical symmetric one where each soliton sits on a spherical cell of radius  $R$  with specific boundary conditions imposed on fields at the surface of the sphere. The configuration of the meson fields, centered at each lattice point, generates a periodic potential in which the quarks move.

The spinor of quark fields must satisfy the Bloch theorem:

$$\psi_{\mathbf{k}}(r) = e^{i\mathbf{k}\cdot\mathbf{r}}\Phi_{\mathbf{k}}(r), \quad (25)$$

where  $\mathbf{k}$  is the crystal momentum (which for the ground state is equal to zero) and  $\Phi_{\mathbf{k}}(r)$  is a spinor that has the same periodicity of the lattice.

### A. Boundary conditions

In the literature various sets of possible boundary conditions have been discussed [18, 19]. In our work we adopt the choice of Ref. [18] which relates the boundary conditions at  $R$  to the parity operation,  $\mathbf{r} \rightarrow -\mathbf{r}$ . Respect to this symmetry the lower component  $v(r)$  of quark spinor and the pion  $h(r)$  are odd, and therefore they have to vanish at  $R$ :

$$v(R) = h(R) = 0. \quad (26)$$

Similarly, for the  $\sigma$  field and the upper Dirac component the argument based on parity provides the conditions:

$$u'(R) = \sigma'_h(R) = 0. \quad (27)$$

The boundary conditions at  $r = 0$  remain the ones given in eq. (15). Basically the calculation consists in solving the set of coupled field equations in a self-consistent way for a given value  $R$ ; practically we start from  $R = 4$  fm, for which the periodic solutions are indistinguishable from the vacuum ones, and we slowly decrease the cell radius down to the smallest radius for which self-consistent solutions can be obtained. The parameter set is the same used for vacuum calculations.

In Fig. 2 we plot the Dirac and the chiral fields for different values of  $R$ ; down to  $R = 2$  fm, the solutions do not change significantly, but as the cell radius shrinks to lower values, we see that all the fields are deeply modified by the finite density. In Fig. 3 we show the results for the total energy of the soliton at mean-field level, in the present model and in the linear  $\sigma$ -model. For each given value of  $m_\sigma$ , the logarithmic model allows the system to reach higher densities. Notice that as  $m_\sigma$  raises, the system remains stable to lower  $R$  because chiral fields are more and more restricted to lay on the chiral circle.

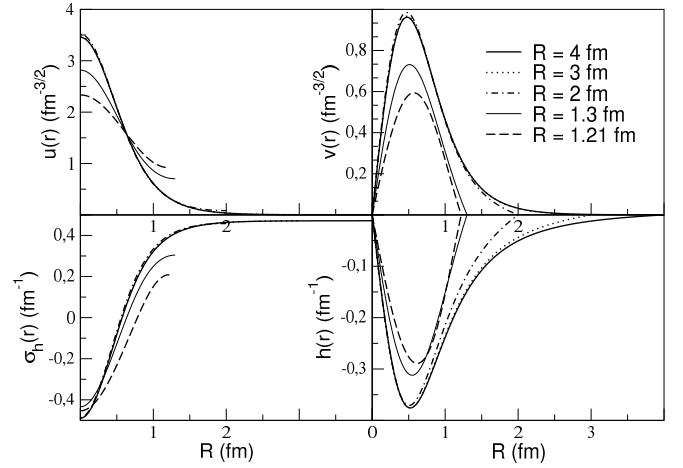


Figure 2: Upper and lower components of the Dirac spinor,  $\sigma$  and pion fields for different values of the cell radius  $R$ .

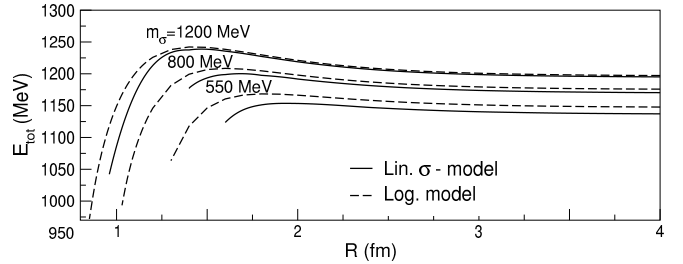


Figure 3: Total energy of the soliton as a function of cell radius  $R$  for the linear  $\sigma$ -model [18] and for the present model. Different values of  $m_\sigma$  are considered.

### B. Band width

We have been solving a problem in which quarks are moving in a periodic potential and therefore Bloch theorem tells us that a band should form. How to define the width of the band is highly not trivial. The most sophisticated technique is the one provided in [18].

Here we adopt two much simpler procedures. The first method is taken from [15], where the authors estimates the band width as:

$$\Delta = \sqrt{\epsilon_0^2 + \left(\frac{\pi}{2R}\right)^2} - |\epsilon_0|, \quad (28)$$

$$\epsilon_{top} = \epsilon_0 + \Delta, \quad (29)$$

where  $\epsilon_0$  is the eigenvalue of the ground state.

An alternative approximation to the band width is obtained, following [16], by imposing that the lower Dirac component vanishes at the boundary:

$$u(R) = 0. \quad (30)$$

In Fig. 4 we plot the quark eigenvalue as a function of the cell radius  $R$ . The line labeled  $\epsilon_{top}^{(a)}$  corresponds to the estimate of the top of the band given by eq. (28),

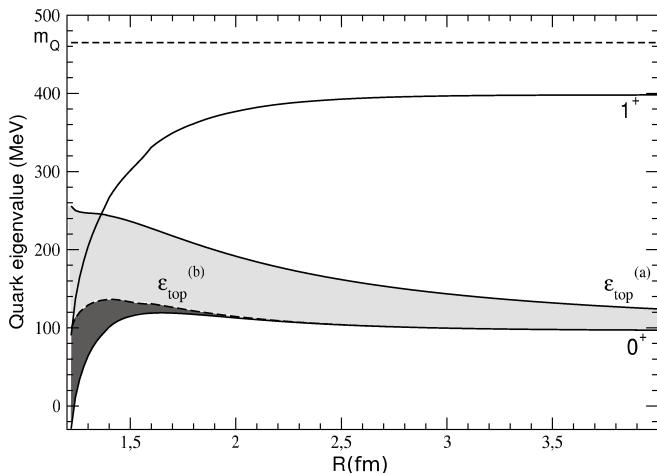


Figure 4: Quark eigenvalue as a function of the cell radius  $R$ . The shaded areas represent the band as estimated in eq. (28) and in eq. (30). We have also included the first excited state  $1^+$ . The quark mass, here 465 MeV, is indicated by the dashed line.

while  $\epsilon_{top}^{(b)}$  follows from eq. (30).

A more accurate evaluation of the band effects can be obtained by solving in a self-consistent way the field equations, which depend also on  $\mathbf{k}$ , as discussed in [18]. There it is shown that  $\epsilon_{top}^{(b)}$  is an upper limit to the top of the band and that the true top lies about half way between this upper limit and the bottom of the band. In conclusion, the band width turns out to be considerably smaller than the one estimated using the first method which leads to the upper limit  $\epsilon_{top}^{(a)}$ .

It has been discussed in the literature how to interpret the results obtained using the Wigner-Seitz lattice and in particular which should be the indications of quark deconfinement. In [15] it has been suggested that deconfinement takes place when the upper band, which corresponds to Grand Spin  $\mathbf{G} = 1$ , merges with the lower band. In our case this occurs roughly at the same density at which the solitonic solutions are lost.

From the results shown in Figs. 4 and 3 it is clear that the simple lagrangian we are discussing does not provide saturation. While it is possible to reach densities higher than  $\rho_0$  by using a large value for  $m_\sigma$ , the total energy always decreases at small  $R$ . A repulsion mechanism is clearly needed.

### C. Observables at finite density

As remarked in the previous section, the results we have obtained have no physical relevance at densities of the order or above nuclear matter saturation density  $\rho_0$ . What is clearly missing is repulsion, which can presumably be provided by the introduction of vector mesons in the model. On the other hand our results can be meaningful at sub-nuclear densities where the dynam-

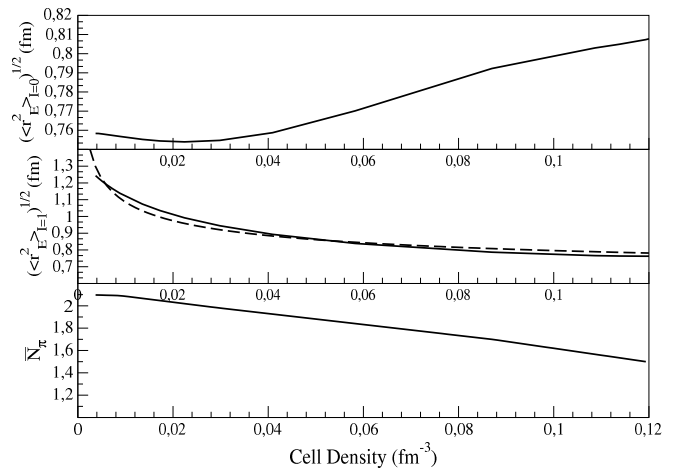


Figure 5: Isoscalar (upper panel), isovector (middle panel) electric radii and average number of pions (lower panel) as a function of cell density  $\rho_C$ . The dashed line represents a function of the density cell of the form of  $a + b\rho_C^{-1/3}$ .

ics is dominated by chiral fields. The question about the modification of the nucleon properties at finite density have been investigated in many analysis, both experimental [28] and theoretical [29–33].

In Fig. 5 we show the isoscalar and isovector electric radius as a function of the spherical cell density. Their expressions read:

$$\langle r_E^2 \rangle_{I=0} = \int_0^R r^4 (u^2(r) + v^2(r)) dr, \quad (31)$$

$$\langle r_E^2 \rangle_{I=1} = \frac{1}{\mathcal{I}} \int_0^R r^4 \frac{8\pi}{3} h^2(r) dr, \quad (32)$$

where  $\mathcal{I}$  is the moment of inertia [34]:

$$\mathcal{I} = \int_0^R r^2 \frac{8\pi}{3} h^2(r) dr. \quad (33)$$

Notice the completely different behaviour we are obtaining for the isoscalar and for the isovector electric radius. The estimate of the latter is, on the other hand, quite questionable when done using the mean-field approximation, since it gets contributions only from the pions. Moreover, since its estimate is a ratio between two quantities having a similar structure (eqs. (32) and (33)) it simply scales with  $R$ , as shown in Fig. 5. The estimate of the isoscalar radius is more robust at mean-field level. The dependence of this quantity on the density has been discussed in several theoretical papers. In our approach, the isoscalar radius shows a slight swelling as the density raises, in agreement with the results obtained in [31–33]. In Fig. 5 we also show the behaviour of the number of pions  $\bar{N}_\pi$  at finite density. The possibility of an enhancement of the pion cloud, when the nucleon is not isolated, has been discussed in the literature [30]. In the present approach we obtain instead a slight decrease of  $\bar{N}_\pi$ .

## VI. CONCLUSIONS

We used a Lagrangian with quarks degrees of freedom based on chiral and scale invariance to study how the soliton behaves in vacuum and at finite density.

To describe the single nucleon properties in vacuum we have used a projection technique. The values of the static observables in the present model are closer to the experimental ones in comparison to the results obtained in the linear  $\sigma$ -model.

For the description of the soliton at finite density we have employed the Wigner-Seitz approximation. *We have shown that the new potential, which includes a logarithmic term originating from the breaking of scale invariance, allows the system, for each given  $m_\sigma$ , to reach densities larger than the ones obtained with the  $\sigma$ -model.*

The main problem of the model discussed in our paper is the absence of saturation, presumably due to the absence of vector mesons. On the other hand, at sub-nuclear densities the dynamics should be dominated by the chiral fields and the modifications of the nucleon observables obtained in our work can therefore be physically relevant in the low-density range. In particular the isoscalar radius presents a slight swelling, of the order of 5%. This trend is in agreement with previous calculations [31–33].

The present work will be extended in several directions. First vector mesons will be included, in order to provide the necessary repulsion at large densities. Next, a more precise and accurate calculation of the band in the soliton crystal will be done following Ref. [18]. Work is in progress in order to study this same model by using the technique developed in Ref. [35], which provides a more precise description of a multi-soliton system. Finally, the model can also be studied at finite temperature, including the dynamics of the dilaton field. We can expect that the effect of the finite temperature on the soliton lattice will be to reduce the stability, by lowering the value of the dilaton field and therefore making it more easy for the chiral fields to fluctuate. It will be interesting to compare the obtained phase diagram with the one proposed by McLerran and Pisarski [10].

## Acknowledgments

It is a pleasure to thank B.Y.Park and V. Vento for many stimulating discussions, M.Birse and J.McGovern for useful comments and tips on calculations.

## APPENDIX

In this Appendix we provide a detailed calculation of the expectation value of the logarithmic potential given in eq. (5) between the projected states (see eq. (22)). As already mentioned and shown in [11], terms which do not

involve the pion field (such as the quark-pion interaction energy and the  $\sigma$  and quark kinetic energies) are not affected by projection. The main issue is the evaluation of the matrix elements of the chiral fields between rotated and unrotated hedgehog states.

These matrix elements for the sigma field  $\sigma(\mathbf{r})$  are:

$$\langle B|\hat{R}(\Omega)^{-1}\sigma(\mathbf{r})^n|B\rangle = \bar{\sigma}(\mathbf{r})^n\langle B|\hat{R}(\Omega)^{-1}|B\rangle, \quad (\text{A.34})$$

where:

$$\bar{\sigma}(\mathbf{r}) = \frac{1}{2} \left( \sigma(\mathbf{r}) + \hat{R}(\Omega)^{-1}\sigma(\mathbf{r}) \right) \equiv \sigma_h(r). \quad (\text{A.35})$$

In an analogous way, for the pion field the matrix elements become:

$$\langle B|\hat{R}(\Omega)^{-1}\boldsymbol{\pi}(\mathbf{r})|B\rangle = \bar{\boldsymbol{\pi}}(\mathbf{r})h(r)\langle B|\hat{R}(\Omega)^{-1}|B\rangle, \quad (\text{A.36})$$

$$\bar{\boldsymbol{\pi}}(\mathbf{r}) = \frac{1}{2} \left( \hat{\mathbf{r}} + \hat{R}(\Omega)^{-1}\hat{\mathbf{r}} \right). \quad (\text{A.37})$$

Since the potential is a function of the pion only through quadratic terms, by using the previous relation we get:

$$\begin{aligned} \langle B|\hat{R}(\Omega)^{-1}\boldsymbol{\pi}^2(\mathbf{r})|B\rangle &= g(\Omega, \theta, \phi)\langle B|\hat{R}(\Omega)^{-1}|B\rangle, \\ g(\Omega, \theta, \phi) &= \frac{1}{2}h(r)^2 \left( 1 + \hat{\mathbf{r}} \cdot \hat{R}(\Omega)^{-1}\hat{\mathbf{r}} \right), \end{aligned} \quad (\text{A.38})$$

where the function  $g$  depends on Euler angles  $\Omega$  and on the polar and azimuthal angles.

For a generic function  $F$  of the quadratic pionic terms, the following relation holds:

$$\langle B|\hat{R}(\Omega)^{-1}F[\boldsymbol{\pi}^2(\mathbf{r})]|B\rangle = F[g(\Omega, \theta, \phi)]\langle B|\hat{R}(\Omega)^{-1}|B\rangle. \quad (\text{A.39})$$

Therefore the projection of the potential term can be obtained by leaving the pure  $\sigma$  terms unchanged and by replacing the quadratic terms of the pion with the function  $g$  given in eq. (A.38):

$$\begin{aligned} V(\sigma_h, h, g(\Omega, \theta, \phi)) &= \\ \lambda_1^2 (\sigma_h^2 + h^2 g(\Omega, \theta, \phi)) - \lambda_2^2 \text{Log} (\sigma_h^2 + h^2 g(\Omega, \theta, \phi)) \\ - \sigma_0 m_\pi^2 \sigma_h. \end{aligned} \quad (\text{A.40})$$

The expectation value of the potential between the projected states, eq. (22), becomes:

$$\begin{aligned} \langle JJ - J| : \int d^3r V(\sigma_h, h, g(\Omega, \theta, \phi)) : |JJ - J\rangle &= \\ \frac{1}{N_J} \int_0^\infty r^2 dr \int_0^\pi \sin \theta d\theta \int_0^{2\pi} d\phi & \\ \times \int d\Omega^3 D_{J,J}^J(\Omega) V(\sigma_h, h, g(\Omega, \theta, \phi)) \langle B|\hat{R}(\Omega)^{-1}|B\rangle & \end{aligned} \quad (\text{A.41})$$

where the Wigner function is equal to:

$$D_{J,J}^J(\Omega) = e^{-iJ(\alpha+\gamma)} \left( \cos \frac{\beta}{2} \right)^{2J}. \quad (\text{A.42})$$

Finally, the overlap between rotated and unrotated hedgehog states reads:

$$\begin{aligned} \langle B | \hat{R}(\Omega)^{-1} | B \rangle = & \\ & \left( \cos \frac{\beta}{2} \cos \frac{\alpha + \gamma}{2} \right)^3 \\ & \times \exp \left( \overline{N}_\sigma + \frac{\overline{N}_\pi}{3} \left( 4 \cos^2 \frac{\beta}{2} \cos^2 \frac{\alpha + \gamma}{2} - 1 \right) \right). \end{aligned} \quad (\text{A.43})$$

Here  $\overline{N}_\sigma, \overline{N}_\pi$  are the average numbers of  $\sigma$  and  $\pi$  mesons in the hedgehog state and  $N_J$  is a normalization integral; explicit expressions of these quantities can be found in [11, 25].

- 
- [1] R. J. Furnstahl and B. D. Serot, Phys. Rev. **C47**, 2338 (1993).
  - [2] E. K. Heide, S. Rudaz, and P. J. Ellis, Nucl. Phys. **A571**, 713 (1994).
  - [3] G. W. Carter and P. J. Ellis, Nucl. Phys. **A628**, 325 (1998).
  - [4] G. W. Carter, P. J. Ellis, and S. Rudaz, Nucl. Phys. **A618**, 317 (1997).
  - [5] G. W. Carter, P. J. Ellis, and S. Rudaz, Nucl. Phys. **A603**, 367 (1996).
  - [6] J. Schechter, Phys. Rev. **D21**, 3393 (1980).
  - [7] A. A. Migdal and M. A. Shifman, Phys.Lett. **B114**, 445 (1982).
  - [8] E. K. Heide, S. Rudaz, and P. J. Ellis, Phys. Lett. **B293**, 259 (1992).
  - [9] L. Bonanno and A. Drago, Phys.Rev. **C79**, 045801 (2009).
  - [10] L. McLerran and R. D. Pisarski, Nucl. Phys. **A796**, 83 (2007).
  - [11] M. Birse, Phys.Rev. **D33**, 1934 (1986).
  - [12] S. Kahana and G. Ripka, Nucl.Phys. **A429**, 462 (1984).
  - [13] J. Aichtzelter, W. Scheid, and L. Wilets, Phys.Rev. **D32**, 2414 (1985).
  - [14] B. Glendenning, N. K., Phys. Rev. **C34**, 1072 (1986).
  - [15] D. Hahn and N. K. Glendenning, Phys. Rev. **C36**, 1181 (1987).
  - [16] M. Birse, J. Rehr, and L. Wilets, Phys.Rev. **C38**, 359 (1988).
  - [17] M. Birse, Prog.Part.Nucl.Phys. **25**, 1 (1990).
  - [18] U. Weber and J. A. McGovern, Phys. Rev. **C57**, 3376 (1998).
  - [19] P. Amore and A. De Pace, Phys. Rev. **C61**, 055201 (2000).
  - [20] M. Abu-Shady and M. Rashdan, Phys.Rev. **C81**, 015203 (2010).
  - [21] M. Fiolhais, J. Urbano, and K. Goeke, Phys.Lett. **B150**, 253 (1985).
  - [22] J. Rafelski, Phys. Rev. **D16**, 1890 (1977).
  - [23] M. C. Birse and M. K. Banerjee, Phys.Rev. **D31**, 118 (1985).
  - [24] B. Golli and M. Rosina, Phys.Lett. **B165**, 347 (1985).
  - [25] E. Ruiz Arriola, P. Alberto, J. N. Urbano, and K. Goke, Nucl. Phys. **A591**, 561 (1995).
  - [26] J. Dethier, R. Goldflam, E. Henley, and L. Wilets, Phys.Rev. **D27**, 2191 (1983).
  - [27] T. S. T. Aly, J. A. McNeil, and S. Pruess, Phys. Rev. D **60**, 114022 (1999).
  - [28] J. Aubert et al. (European Muon Collaboration), Phys.Lett. **B123**, 275 (1983).
  - [29] P. Mulders, Phys.Rept. **185**, 83 (1990).
  - [30] M. Ericson and M. Rosa-Clot, Phys.Lett. **B188**, 11 (1987).
  - [31] D.-H. Lu, K. Tsushima, A. W. Thomas, A. G. Williams, and K. Saito, Phys.Rev. **C60**, 068201 (1999).
  - [32] J. R. Smith and G. A. Miller, Phys.Rev. **C70**, 065205 (2004).
  - [33] L. S. Celenza, A. Rosenthal, and C. M. Shakin, Phys. Rev. Lett. **53**, 892 (1984).
  - [34] T. D. Cohen and W. Broniowski, Phys.Rev. **D34**, 3472 (1986).
  - [35] B.-Y. Park, H.-J. Lee, and V. Vento, Phys.Rev. **D80**, 036001 (2009).